# STUDY ON
# CLOUD TOP PRESSURE DEVELOPMENT FROM SENTINEL-3 OLCI OCTPO2

## Algorithm Product Validation and Evolution Report

Issue 2.0, 20.06.2021
EUM/CO/19/4600002221/AIBo

prepared by
Jürgen Fischer and Rene Preusker

| Document, Version | Date | Changes | Originator |
|---|---|---|---|
| VER, v1.0_template | 01.09.2019 | Template | Jürgen Fischer, Rene Preusker |
| VER v1.0 | 18.04.2021 | Original | Jürgen Fischer, Rene Preusker |
| VER v1.1 | 10.05.2021 | | Jürgen Fischer, Rene Preusker, Andi Walther |
| VER v2.0 | 20.06.2021 | Response on comments from EUMESTSAT | Jürgen Fischer, Rene Preusker |

# Table of Content

## Acronyms and Abbreviations

| | |
|---|---|
| AOPC | Atmospheric Observation Panel for Climate |
| AOT | Aerosol Optical Thickness |
| COT | Cloud optical thickness |
| CTP | Cloud-top pressure |
| dof | degrees of freedom |
| Envisat | ESA satellite (see http://envisat.esa.int/) |
| EO | Earth Observation |
| ESA | European Space Agency (http://www.esa.it/export/esaCP/index.html) |
| EUMETSAT | European Organisation for the Exploitation of Meteorological Satellites |
| FUB | Free University Berlin |
| FoV | Field of View |
| GCOS | Global Climate Observing System |
| GEOSS | Global Earth Observing System of Systems |
| GEWEX | Global Energy and Water Exchanges Project |
| GNSS | Global Navigation Satellite System |
| GPS | Global Positioning System |
| HITRAN | High-resolution transmission molecular absorption database |
| IR | Infrared |
| ISCCP | GEWEX International Satellite Cloud Climatology Project |
| TCWV | Total Column Water Vapour |
| L1/L2 | Level 1 / Level 2 |
| LBL | Line-by-line |
| LUT | Look-up table |

| | |
|---|---|
| MERIS | Medium Resolution Imaging Spectrometer Instrument (http://envisat.esa.int/) |
| MODIS | Moderate Resolution Imaging Spectroradiometer (on board the NASA EOS-Aqua satellite) |
| MOMO | Matrix Operator Modell |
| MSG, MTG | METEOSAT Second / Third Generation |
| MWR | Microwave Radiometer |
| NASA | National Aeronautics and Space Administration |
| NIR | Near Infrared |
| NWP | Numerical Weather Prediction |
| OE | Optimal estimation |
| OLCI | Ocean and Land Colour Instrument onboard Sentinel-3 |
| QA4EO | Quality assurance framework for earth observation |
| RTC / RTM | Radiative Transfer Code / Model |
| RTTOV | Radiative Transfer for TOVS (TIROS Operational Vertical Sounder) |
| SoW | Statement of Work |
| SWIR | Shortwave Infrared |
| TCWV | Total Column Water Vapour (=TCWV) |
| TIR | Thermal Infrared |
| TIROS | Television and InfraRed Observation Satellite |
| TOA | Top of atmosphere |
| TPW | Total Precipitable Water (=TCWV) |
| VIS | Visible/solar part of the spectrum |
| WMO | World Meteorological Organization |
| WMO UR | WMO User Requirements |
| 1Dvar | 1 Dimensional Variational |

**Applicable Documents**

| [AD-1] | Generic Statement of Work for Product Evolution/Development Studies | *EUM/TSS/SOW/17/930252* |
|--------|----------------------------------|------------------------|
| [AD-2] | Sentinel-3 Mission Requirements Traceability Document | *Donlon, C., EOP-SM/2184, CD-cd, Issue 1, 2011* <br> *http://download.esa.int/docs/EarthObservation/GMES_Sentinel-3_MRTD_Iss-1_Rev-0-issued-signed.pdf* |
| [AD-3] | The Global Monitoring for Environment and Security (GMES) Sentinel-3 mission | *Donlon, C., B. Berruti, A. Buongiorno, M.-H. Ferreira, P. Femenias, J. Frerick, P. Goryl, U. Klein, H. Laur, C. Mavrocordatos, J. Nieke, H. Rebhan, B. Seitz, J. Stroede, R. Sciarra, Rem. Sens. Env., 120, 37-57, 2012* |

**Reference Documents**

| [RD-1] | Cloud Top Pressure Algorithm Product Validation and Evolution Report | *Jürgen Fischer, Rene Preusker, Ulrich Küster, Cintia Carbajal-Henken; Report of ESA SEOM "Advanced Clouds, Aerosols and WAter vapour products for Sentinel-3/OLCI" project, 2017.* |
|--------|----------------------------------|------------------------|
| [RD-2] | Sentinel-3A Product Notice – OLCI Level-2 Ocean Colour | *https://www.eumetsat.int/website/home/Data/CopernicusServices/Sentinel3Services/ Ocean Colour/index.html* |
| [RD-3] | Advanced Clouds, Aerosols and WAter vapour products for Sentinel-3/OLCI (CAWA) | *https://earth.esa.int/web/ sppa/activities/cawa/ projects-documents* |
| [RD-4] | Technical Note: Sentinel-3 OLCI-A spectral response functions | *Sentinel 3 CalVal Team, S3-TN-ESA-OL-660, issue 2.0,https://www.eumetsat.int/website/home/Data/CopernicusServices/Sentinel3Services/Ocean Colour/index.html, 2016.* |
| [RD-5] | Sentinel-3 User Handbook | *https://sentinels.copernicus.eu/documents/247904/ 685236/Sentinel-3_User_Handbook* |
| [RD-6] | Land Surface Pressure Estimate from Measurements in the Oxygen A Absorption Band | *Breon, F.M., & Bouffies, S., Jour. of Applied Meteorology, Vol. 35, p. 69, 1996* |
| [RD-7] | Detection of Cloud-Top Height from Backscattered Radiances within the Oxygen A-Band - Part 1: Theoretical Study | *Fischer, J., and Grassl, H., J. Appl Met., Vol. 30, p. 1245, 1991* |
| [RD-8] | Inverse Methods for Atmospheric Sounding: Theory and Practice | *Rodgers, C., World Scientific, London, 2000.* |
| [RD-9] | Study on O2 band Cloud Top Pressure retrieval with METimage, Final report | *HYGEOS, Laboratoire d'Optique Atmospherique, universite de Lille/Sciences et technologies, EUMETSAT Reference: EUM/CO/14/4600001448/PDW.* |

# 1   Introduction

This document provides information on the validation of the OLCI *cloud top pressure* retrieval as defined within EUMETSAT's '*Cloud Top Pressure development from Sentinel-3 OLCI*' project OCTPO2.

The 1D-var algorithm estimates cloud top pressure, cloud optical thickness, cloud geometrical thickness and the centre of gravity as well as an uncertainty for each retrieval. The instrument characteristics of Sentinel-3/OLCI as well as atmospheric properties, relevant for the cloud properties retrieval, are discussed with a view to validation of the cloud products.

The satellite Earth-observing spectrometer OLCI onboard Sentinel-3 is introduced and discussed with respect to the task of developing a cloud top pressure retrieval using OLCI's O2 A-band channels in the corresponding ATBD of this project (see Preusker and Fischer, 2021).

The upward top of atmosphere radiance within the spectral domain of OLCI's O2 A-band channels are shown in Figure 1. The OLCI channels 13, 14, and 15 are selected to support the cloud detection and to enable the retrieval of cloud properties, mainly the cloud top pressure. There are hundreds of absorption lines within the O2 A-band but also a few Fraunhofer lines are clearly seen. The nominal response functions of OLCI O2 A-band channels 13, 14, and 15 as well as the reference channels 12 and 16, which are not or not significantly affected by oxygen absorption lines, are plotted as well.
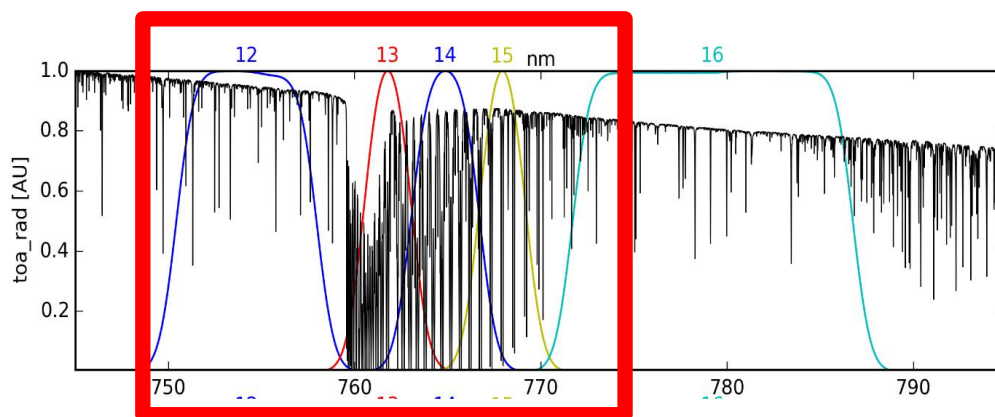


*Figure 1: Upward top of atmosphere radiance via wavelength; The response functions of the O2 A-band OLCI channels 13, 14, and 15 as well as the reference channels 12 and 16 are plotted.*

# 2   Cloud Properties Product Validation

The validation of the OCTPO2 cloud products, cloud top pressure, cloud optical thickness, cloud geometrical thickness, cloud base pressure, and center of gravity is challenging and will be tackled utilizing ground-based, airborne and satellite measurements.

Before we describe the results of the validation exercises, we shortly explain relevant parts of the OCTPO2 retrieval scheme (see ATBD for further details: Preusker and Fischer, 2021). The crucial and central part of the cloud top pressure retrieval is the *forward operator*, a module that calculates for a given state of atmosphere and surface the OLCI measurements. To reduce computational effort, we are using look-up tables and interpolations therein, which are based on accurate radiative transfer simulations for the used OLCI bands considering surface reflectivity spectra, surface pressure,

atmospheric temperature profiles and vertical profiles of the cloud optical and microphysical properties.

Principally all data that are crucial for the cloud properties retrieval need to be considered in the simulation, but even in complex air-borne campaigns it is impossible to measure all information on the vertical profiles of the cloud optical and microphysical properties. Further it is impossible to prepare and perform all radiative transfer simulations to express the total possible variability of a profile, e.g., independent values in each layer, as independent parameters in a LUT, since the size of these tables would grow very rapidly with an increasing number of parameters (*the curse of* dimensionality). This problem can and must be mitigated by using dimensionality reduction techniques.

The profile of cloud extinction is not accessible from the few O2 channels of OLCI, thus, the degrees of freedom must be reduced to a smaller parameter state space. In addition to the cloud top pressure and the cloud optical thickness, we are using only two further parameters to describe the vertical structure of the cloud: the cloud geometrical thickness CGT and the center of gravity COG (the first moment of the vertical distribution of extinction) as shown in Figure 2, assuming a triangular shape of the extinction profile. This is simple enough to be tackled by the low amount of information of an OLCI observation. CGT and COG are parametrized by numbers between 0 and 1. This modus operandi has two other advantages: first it reflects partly the experimental findings for ice and water clouds, and second it provides differentiable parameters, advantageous for optimal estimation.

The simulations to generate the LUTs were performed using the Matrix Operator Model (MOMO, Hollstein and Fischer, 2012). The absorption due to atmospheric gases, namely oxygen, has been calculated by using HITRAN 2016, updated by Drouin et al. (2017). The k-bins are estimated by using the approach from Doppler et al. (2013) and updated by Preusker and Fischer (2019). The radiances were calculated for different solar zenith angles (SZA), viewing zenith angles (VZA), relative azimuth angles (RAA), surface reflectances, cloud optical thicknesses, vertical profiles, and spectral characteristics of the bands. Water surfaces are simulated with a fixed wind speed of $v$=7m/s taken the Cox and Munk (1954) wave slope distribution into account. Above land surfaces a Lambertian reflector is assumed with reflectance values between $\alpha$=0.0 and $\alpha$=0.95 in steps of $\Delta\alpha$=0.05.
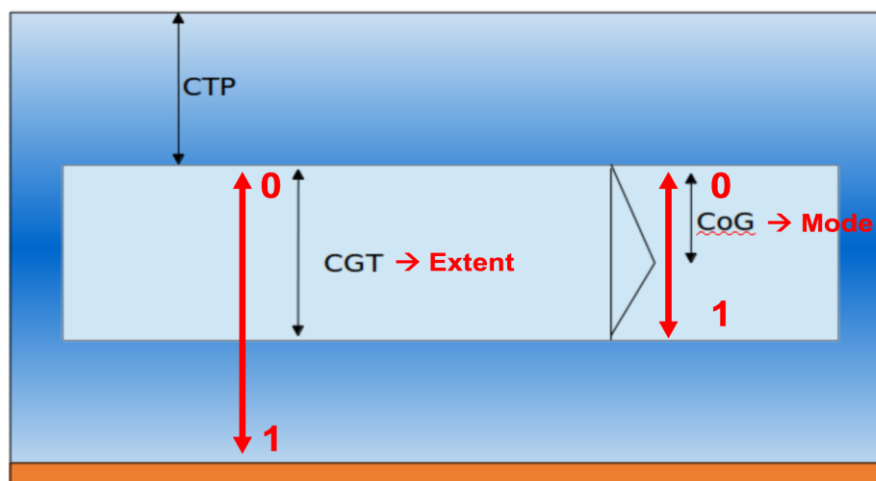


*Figure 2: Cloud top pressure CTP, cloud geometrical thickness CGT, and center of gravity CoG.*

For the validation of the OCTPO2 cloud products we used ground-based observations, airborne and satellite measurements. The cloud-radar, micropulse and ceilometer measurements at the SGP ARM-site provide comprehensive cloud observations which are taken for a comparison with the OLCI OCTPO2 cloud products. In the framework of the EUREC[4]A cloud campaign in 2020, dedicated flights above the Caribbean with a lidar have been performed. As a third exercise, we compared cloud

properties, derived from MODIS measurements, which fly onboard the Terra and Aqua satellite, with the OCTPO2 retrievals.

## 2.1  Validation of OLCI Cloud Properties with Air-borne Lidar Measurements

Airborne-based validation studies of cloud top pressure products, which are derived from satellite observations, are challenging due to the temporally and spatially high variable clouds. However, there are dedicated airborne campaigns, such as the field campaign EUREC[4]A for the validation of the OCTPO2 cloud products (Bony et al., 2017).

During the EUREC[4]A HALO airborne campaign, which last from the 19th of January to the 18th of February 2020, there have been 15 flights (see Table 2). The German high-altitude and long-range research aircraft HALO is a modified Gulfstream G550 business jet with a long endurance (more than 10 flight hours), a long-range (about 8000 km), and a high ceiling (15.5 km) (Wendisch et al. 2016). In cooperation with the DLR and the Universities of Cologne, Hamburg, Leipzig, and Munich, it was equipped with an extensive set of remote sensing instrumentation including: the differential absorption and high-spectral-resolution lidar system (WALES, Water vApour Lidar Experiment in Space), HAMP (the HALO Microwave Package) which includes the cloud radar MIRA36 (36 GHz) and a microwave radiometer, the spectral imager specMACS, and an instrument system that measures spectrally resolved upward and downward solar radiances and irradiances (SMART). The payload also includes in situ measurements of the meteorological properties along the flight track (BAHAMAS), and the ability to launch dropsondes using the AVAPS system (for more details see Bony et al., 2017). The most interesting instrument for the validation of OCTPO2 products are WAVES and MIRA36, however, so far only WALES measurements are available.

The lidar system WALES is a combined differential absorption and high-spectral-resolution lidar (HSRL) system developed and built at DLR (Wirth et al., 2009). WALES is capable of nearly simultaneously emitting four wavelengths, three online and one offline, in the water vapour absorption band between 935 and 936 nm. The three online wavelengths achieve the necessary sensitivity needed for measurements over the whole range of tropospheric water vapour concentration. The vertical resolution of the raw data is 15 m. In addition to the 935-nm channel, the receiver is equipped with polarization-sensitive aerosol channels at 532 and 1064 nm, the first one with high-spectral-resolution capabilities using an iodine filter in the detection path (Esselborn et al. 2008). This allows for collocated measurements of humidity, optical depth, clouds, and aerosol optical properties.

*Table 2: HALO flight days and flight duration during EUREC4A, data used for validation are in green.*

| Datum | OLCI | time (UTC) | HALO | time (UTC) | comments |
|-------|------|------------|------|------------|----------|
|       |      |            |      |            |          |
| 19.01.2020 | A, B | 14:13.56 – 14:16.56 | transect | 09:33 – 18:48 | No WALES data so far |
| 22.01.2020 | B | 13:56.49 – 13:59.49 | circle | 14:56 – 19:34 | No overpass |
| 24.01.2020 | A | 13:44.01 – 13:47.01 | circle | 09:29 – 18:41 | |
| 26.01.2020 | B | 13:53.04 – 13:56.04 | circle | 12:05 – 21:21 | |
| 28.01.2020 | A | 13:40.17 – 13:43.17 | circle | 16:12 – 23:00 | No overpass |
| 30.01.2020 | B | 13:49.19 – 13:52.19 | circle | 11:19 – 15:09 | |
| 31.01.2020 | A | 14:02.43 – 14:05.43 | circle | 14:07 – 00:10 | No overpass, lidar starts |
|  | B | 13:23.08 – 13:26.08 |  |  | 15:30 |
|  |  |  |  |  |  |
| 02.02.2020 | B | 14:11.45 – 14:11.45 | circle | 11:28 – 20:15 | too far west |
| 05.02.2020 | A | 13:32.48 – 13:35.48 | circle | 09:15 – 18:20 | |
| 07.02.2020 | A | 14:21.25 – 14:24.25 |  |  | |
|  | B | 13:41.50 – 13:41.50 | circle | 12:00 – 21:11 | |
| 09.02.2020 | A | 13:29.04 – 13:32.04 | circle | 09:35 – 18:02 | |
| 11.02.2020 | A | 14:17.41 – 14:20.41 |  |  | too far west |
|  | B | 13:38.06 – 13:41.06 | circle | 12:29 – 21:37 | |
| 13.02.2020 | A | 13:25.19 – 13:28.19 | circle | 07:56 – 17:18 | |
| 15.02.2020 | A | 14:13.56 – 14:16.56 | circle | 15:06 – 24:12 | No overpass |
|  | B | 13:34.22 – 13:37.22 |  |  | |
| 18.02.2020 | A, B |  | transect |  | No WALES data so far |

For the validation of the OCTPO2 cloud products, namely the cloud top pressure we used the WALES cloud top height which we converted into cloud top pressure, using the surface pressure and the surface temperature as provided in the OLCI data files. The WALES cloud top height is delivered with the coordinates (latitude and longitude) and time of the measurements. These data are used to collocate the OLCI and WALES measurements, whereby the cloud top height products are averaged over a distance of roughly 300 m, the spatial resolution of OLCI. The used OLCI Data is full resolution, non time-critical, L1B, and L2 (for the cloud mask), provided by EUMETSAT Sentinel data-hub (CODA). No further auxiliary data is used.

The two photos, taken from the HALO on the 24th of January 2020, 11:58 (left) and one hour later at 12:59, demonstrate the variability of clouds in the overserved region (*Figure 3*).



*Figure 3: Photos, taken from the HALO on 24th of January 2020, 11:58 (left) and one hour later at 12:59 (taken from HALO flight report, B. Stevens, 2020).*

There was an overflight of Sentinel-3A on the 24th of January 2020, which takes from 13:44.01 to 13:47.01 UTC to observe the study area. The derived OCTPO2 cloud top pressure is shown in *Figure 4*. The white circle indicates the flight track of HALO, which flew in a clockwise direction. The white arrow points to the location where HALO was during the overpass. The geometrical size of the clouds varies significantly, some clouds are only a few 100 meters in diameter, others have dimensions of more than 100 km. With a spatial resolution of 260*300 m$^2$, even small cumulus clouds are detected. The estimated CTP varies from 950 to less than 500 hPa. The CTP values of the small-scale cumulus clouds are between 950 to 850 hPa.

*Figure 5* shows the cloud top pressure products derived from OLCI, whereby the standard deviation within 3*3 OLCI pixels is indicated as bars to illustrate the small-scale CTP variability, as well as from WALES-Lidar on the 24th of January 2020. The overpass of Sentinel-3 was at 13:44 UTC. The CTP products are displayed for a complete HALO circle, which takes roughly one hour. Since clouds change during ± 30 minutes of the overpass, we mainly compare the variability of the different cloud fields, assuming that the general characteristics of the cloud fields do not change significantly. Both cloud top pressure products, derived from airborne LIDAR and satellite OLCI measurements, are within the same range and partly agree very well, e.g., within the period 14.1 to 14.2 UTC where the decrease and increase of both CTP products are very close.

The cloud base pressure CBP is derived from the OCTPO2 product CGT (cloud geometrical thickness) following:

$$CBP = CTP + (SPR-CTP) * CGT$$

with the surface pressure SPR, provided by the OLCI auxiliary data (ECMWF).
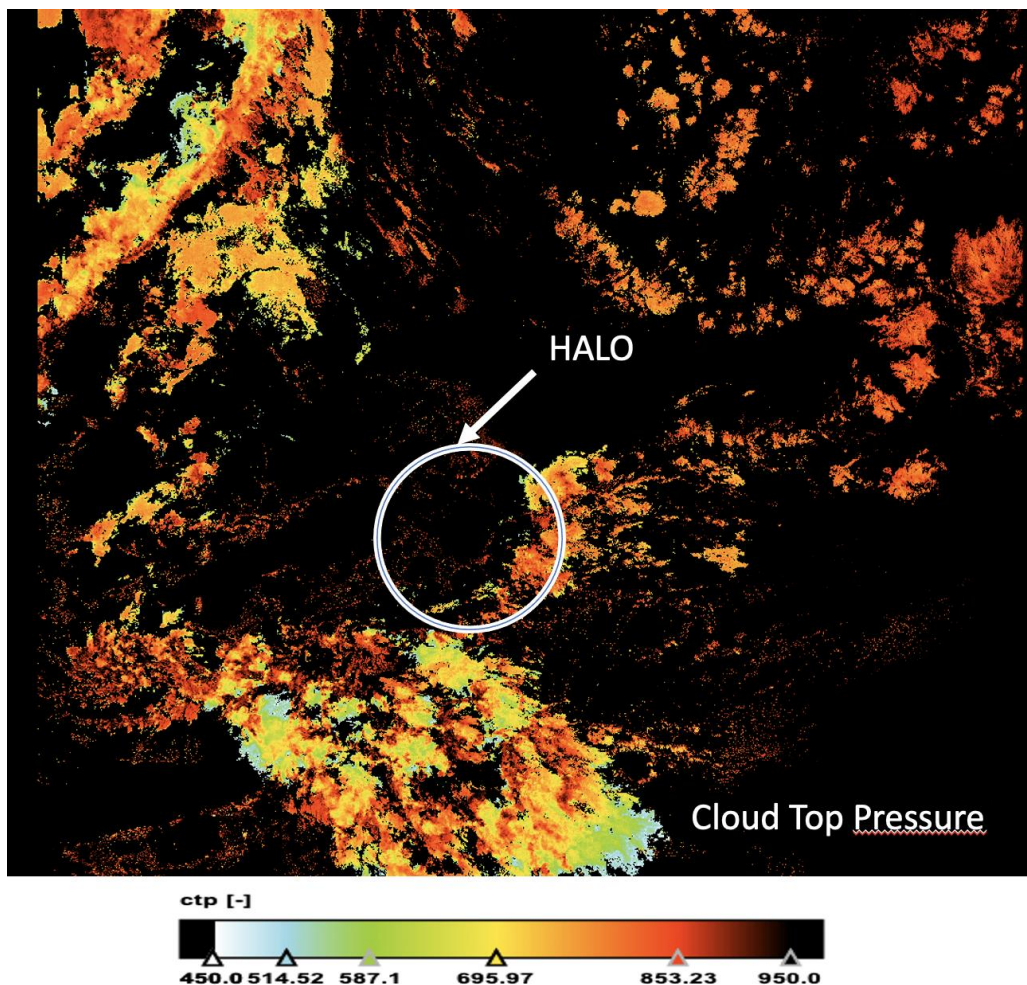


*Figure 4: Cloud top pressure in [hPa], derived from Sentinel-3A, OLCI on the 24th of January 2020 at 13:44 UTC; a white circle indicates the flight track of HALO, which flew in a clockwise direction; white arrow points to the location where HALO was during the Sentinel-3A overflight.*
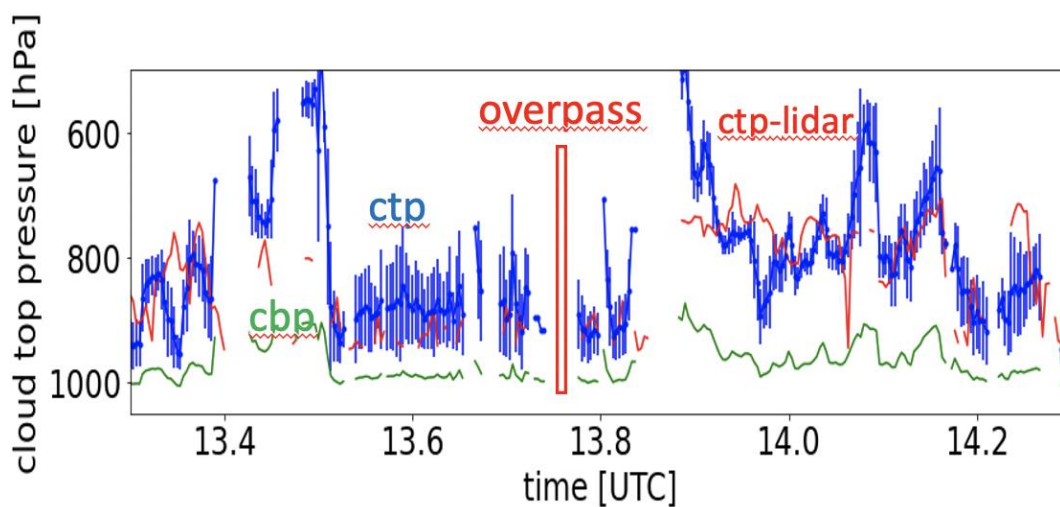


*Figure 5: Cloud top pressure products derived from OLCI (blue), whereby std. deviation within 3\*3 OLCI pixels is indicated as bars, and WALES-Lidar (red) on the 24th of January 2020; the overpass of Sentinel-3 is indicated as a red bar at 13:44 UTC; cloud base pressure as also derived from OLCI (green).*

The quality of the cloud base pressure product depends directly on the uncertainty of the estimated cloud geometrical thickness, which is generally high, since OLCI's $O_2$ A-band channels contain only a little information on the cloud extension, as we discuss in the estimation of the degree of freedom of the OLCI measurements below in more detail.

The cloud optical thickness (COT) and the centre of gravity (COG) are additionally plotted in *Figure 6*. A comparison of COT and the difference of OLCI and Lidar-derived CTP points to the fact that the difference between both retrievals is larger when the COT is below 3, such as seen at 13.9 UTC. The centre of gravity (CoG) does not change significantly and is more or less constant in this case, however, CoG~0.2 is a realistic value for cumulus clouds with an adiabatic droplet growth. The cloud base pressure (CBP) decreases, often together with decreasing CTP. The accuracy of the retrieved CBP depends on the accuracy of the CTP and the CGT retrieval, whereby the later is less reliable because of the limited information content of OLCI's O2 A-band measurements. The degree of freedom DoF varies only between 1.9 and 2.1 within the studied area, which is expected for the type of observed clouds. The CTP retrieval seems to be more reliable, a better match between airborne and satellite-based CTP retrievals, when the COT exceeds a value of 2 (see *Figure 6*). However, also in cases of high COT the comparison shows larger differences when not the same cloud is observed in a field of varying cloud pattern.
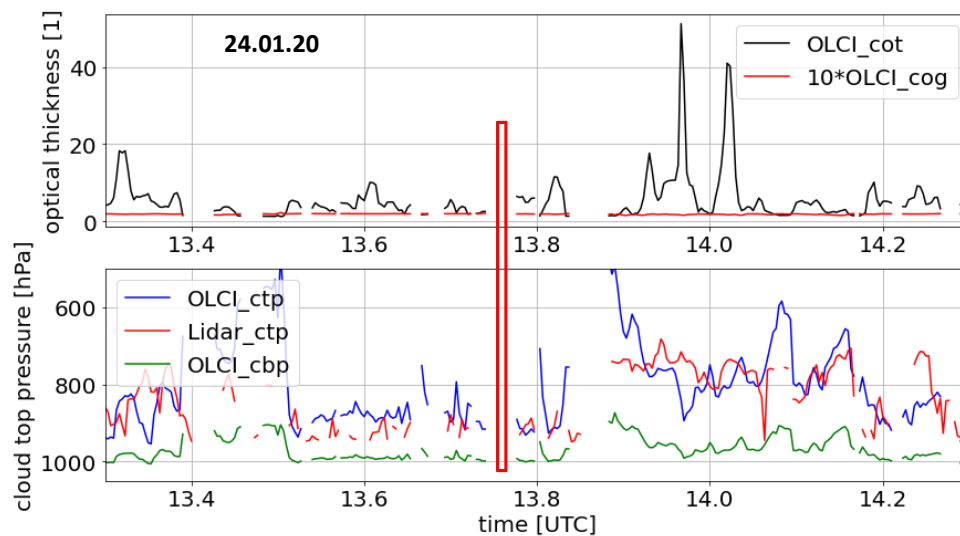


*Figure 6: Cloud top pressure (blue) and cloud base pressure (green) products derived from OLCI and WALES-Lidar (red) (lower Figure), cloud optical thickness and center of gravity as derived from OLCI (upper Figure) on the 24th of January 2020; the overpass of Sentinel-3 is indicated as a red bar at 13:44 UTC.*

Three more comparisons of satellite OLCI and airborne WALES lidar-based cloud top pressure products are shown in Figure 7. On the 26th of January only a few measurements agree, which might be caused by the dominated presence of scattered clouds. There are larger gaps of cloud top height observations from WALES-lidar, which leads to the difficulty to find matchups of OLCI and WALES measurements. On the 30th of January clouds between 740 hPa and 940 hPa are estimated from OLCI and WALES data, however, the agreement is less good when COT is smaller.
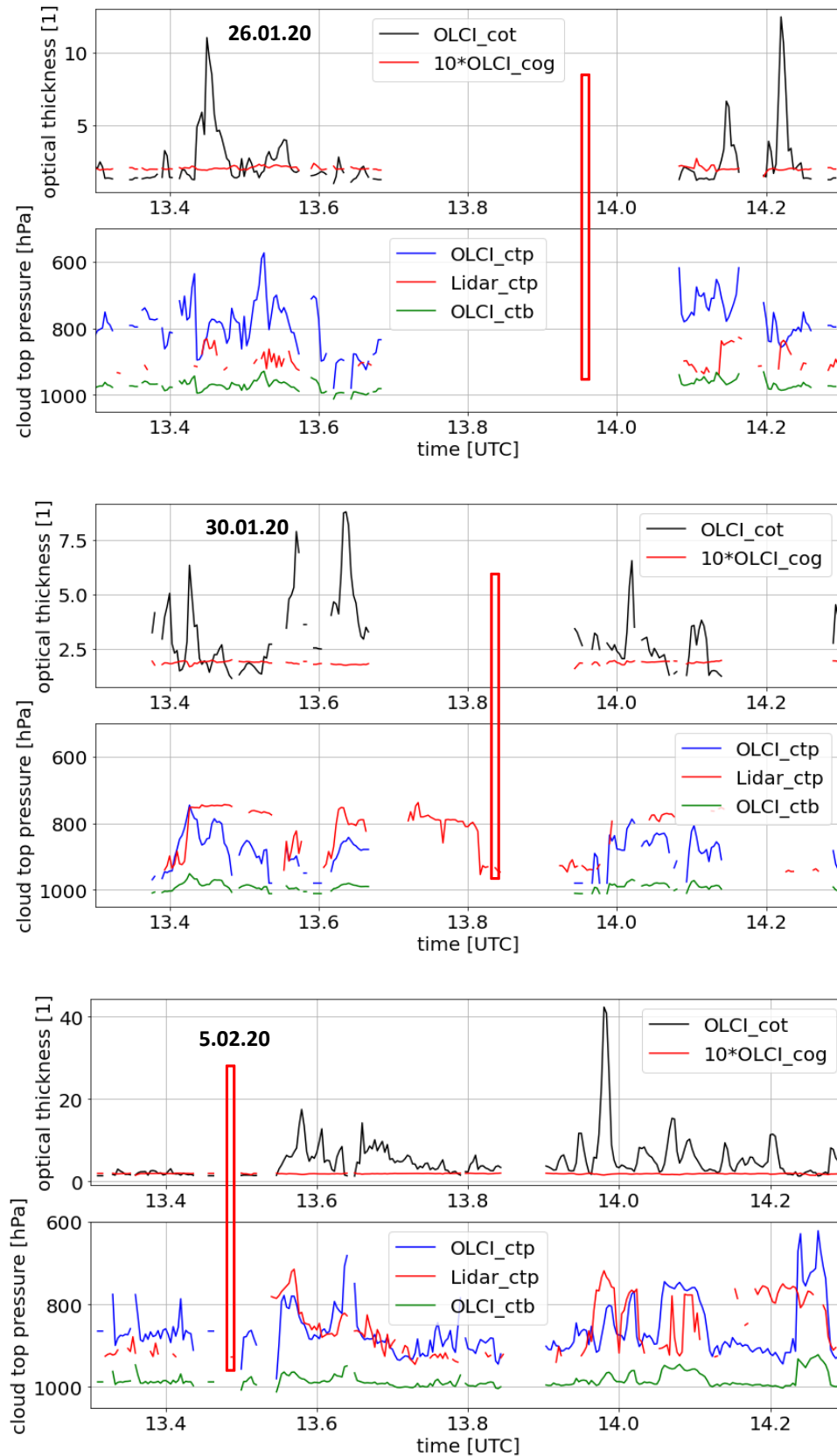
**Figure 7**: *Cloud top pressure (blue) and cloud base pressure (green) products derived from OLCI and WALES-Lidar (red) (lower Figure), cloud optical thickness and center of gravity as derived from OLCI (upper Figure) on the 26th Jan. (upper block), 30th Jan. (middle block), 5th Feb. (lower block) 2020; the overpass of Sentinel-3 is indicated as a red bar.*

Different cloud types with small-scale cumulus and horizontally outspread clouds are observed on the 5th of February, which is shown in Figure 7 (lower part) and Figure 8. The increase in CTP is consistently estimated from OLCI and WALES measurements, such as the increase in CTP from 760 hPa to 900 hPa after 10 minutes and even after 40 minutes of OLCI's overpass.

Assuming that the observed cloud fields might not change too much within the 60 minutes of a HALO circle, the comparison of OLCI and WALES cloud products has been performed. However, the high variability of cloud sizes in terms of horizontal spread can be seen in *Figure 8*. The white circle illustrates the flight track of HALO, but it also shows the difficulty to catch the same cloud from satellite OLCI and airborne WALES measurements.
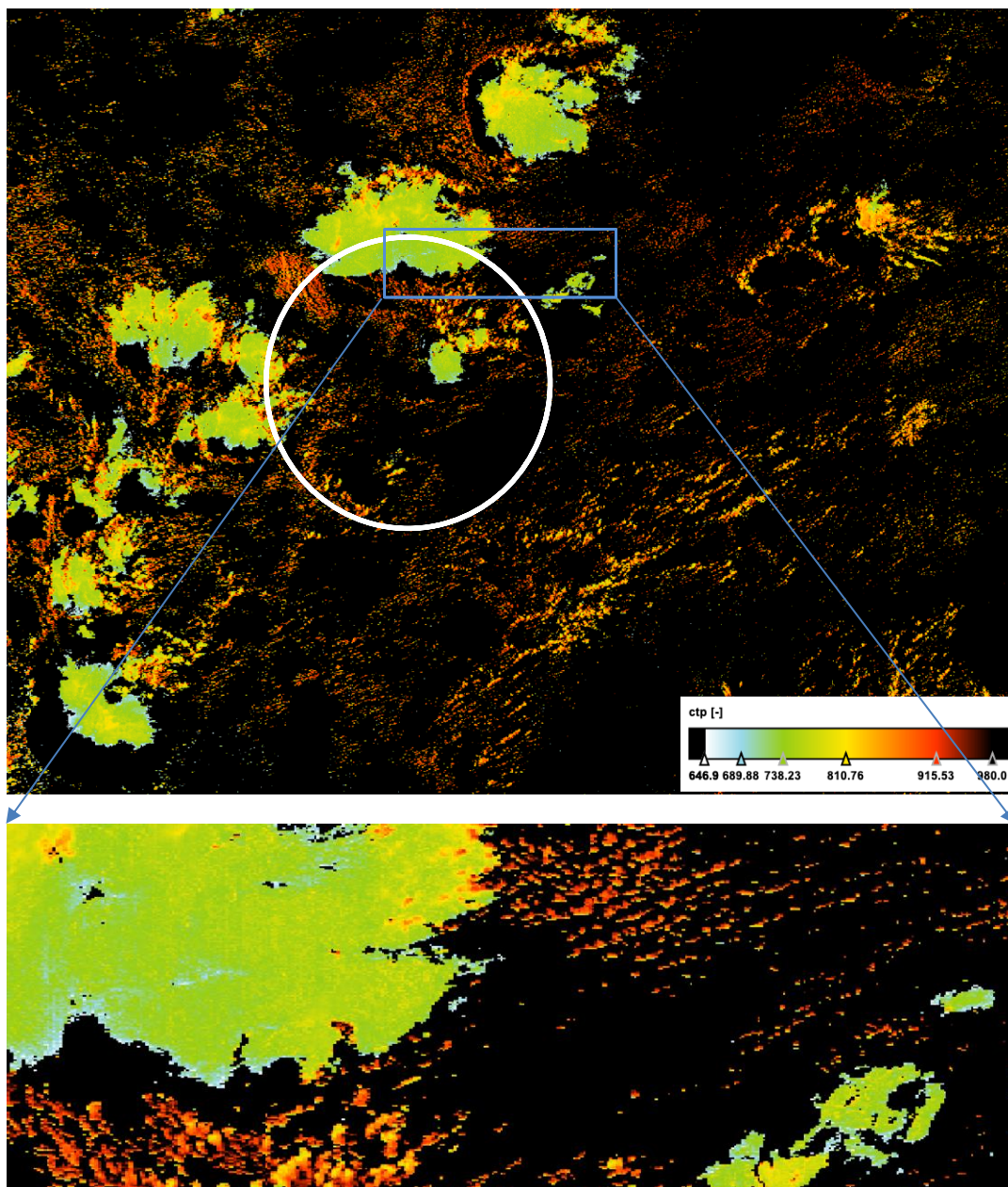


*Figure 8: Cloud top pressure in [hPa], derived from Sentinel-3A, OLCI on the 5th of Feb. 2020 at 13:44 UTC; white circle indicates the flight track of HALO, which flew in a clockwise direction; white arrow points to the location where HALO was during the Sentinel-3A overflight (upper Figure); blue box indicated zoomed area (lower Figure).*
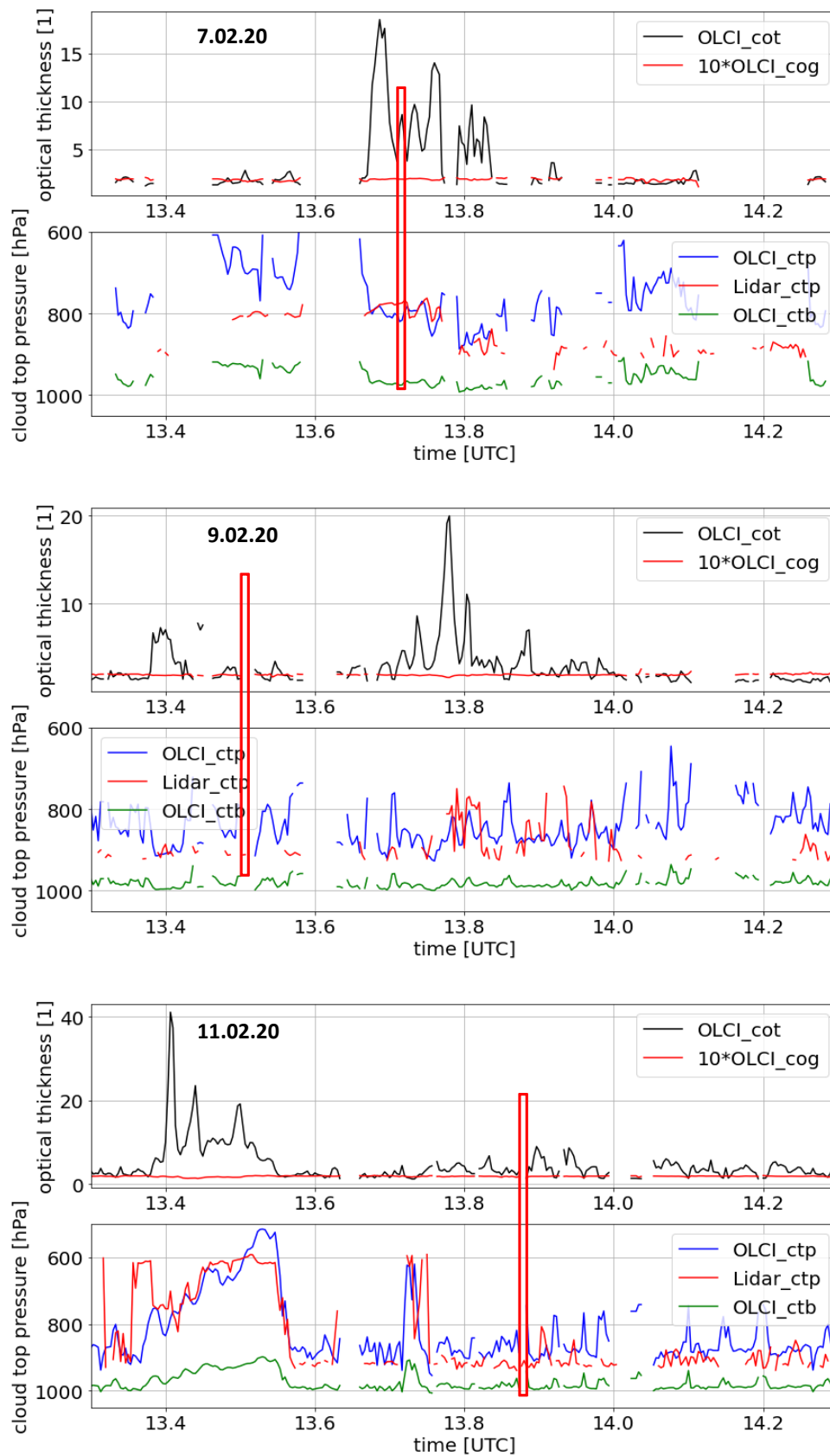
*Figure 9: Cloud top pressure (blue) and cloud base pressure (green) products derived from OLCI and WALES-Lidar (red) (lower Figure), cloud optical thickness and center of gravity as derived from OLCI (upper Figure) on the 7th Feb. (upper block), 9th Feb. (middle block), 11th Feb. (lower block) 2020; the overpass of Sentinel-3 is indicated as a red bar.*

Even clouds of a pixel size of 260*300 m$^2$ could be observed within the expected range of cloud top pressure, but in the case of low optical thickness, which is also due to partly filled pixels, the estimated CTP is too low. This occurs mainly at cloud edges, obvious by the blueish coloured parts. There is no atmospheric process that supports such observation, however, from the radiative transfer processes in the O2 A-band we know that in cases of low atmospheric optical thickness we estimate a lower CTP.

There are more comparisons of satellite OLCI and airborne WALES lidar-based cloud top pressure products from the 7th, 9th and 11th of February which have been studied. All three cases support the previous findings, that the cloud top pressure variability could be well described when compared to WALES lidar-based CTP (see Figure 9).
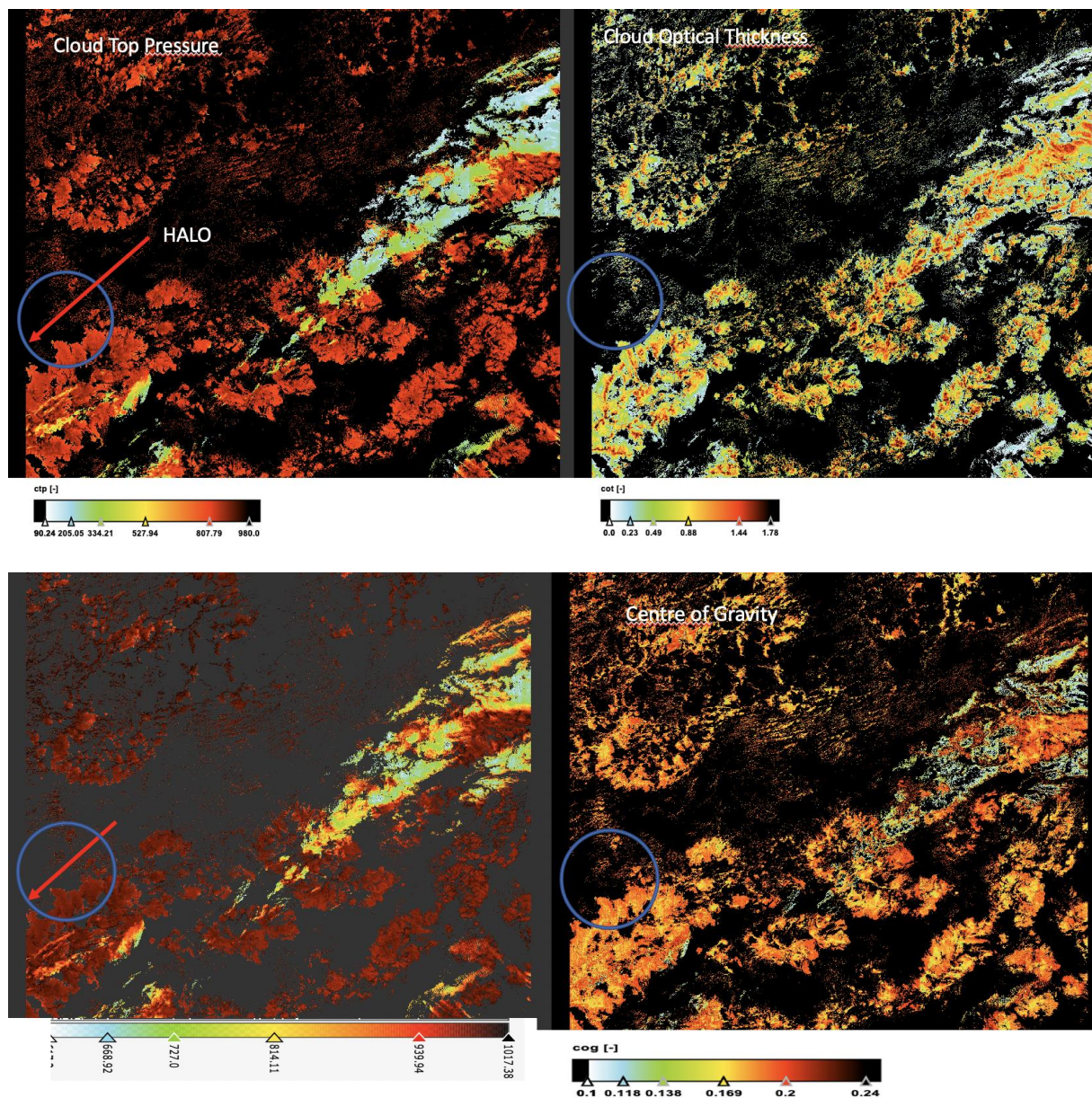


*Figure 10a: Cloud top pressure (upper left), cloud base pressure (lower left), cloud optical thickness (upper right) and center of gravity (lower right) as derived from OLCI on the 13th of Feb. 2020 at 13:25 UTC; the flight track of HALO is indicated as a blue circle.*
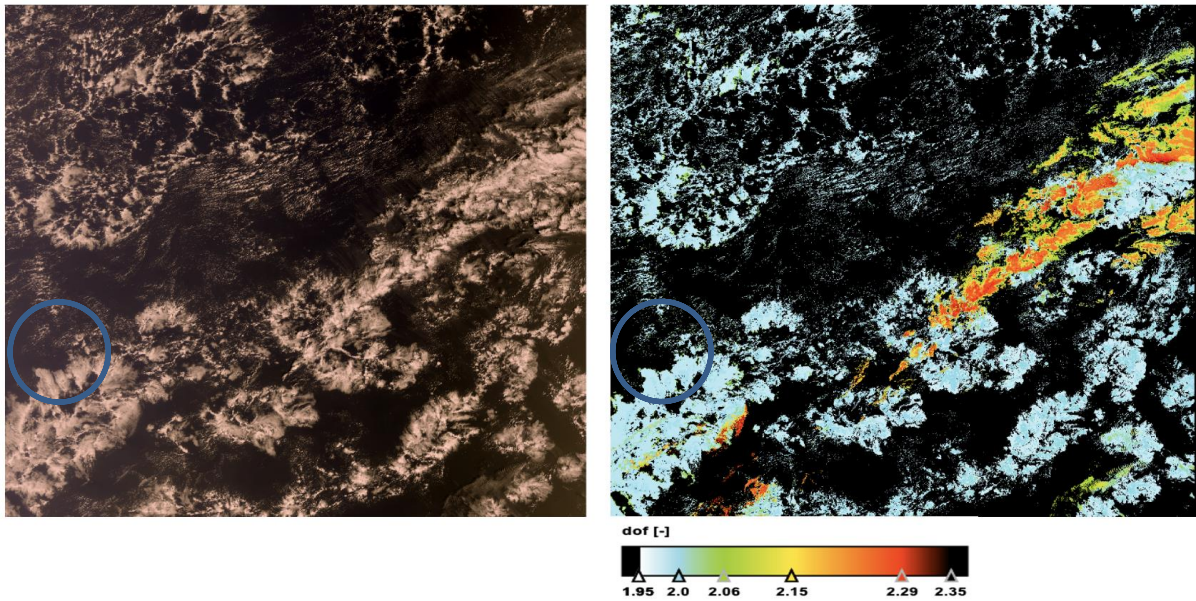
*Figure 10b: As Figure 10a, but for RGB and degree of freedom DoF; HALO flight track in blue.*

On the 13th of February there have been larger extended clouds as well as small-scale cumulus (see Figure 10b). To study the different cloud fields, we display images of the cloud top pressure, the cloud optical thickness, the cloud base pressure and the centre of gravity in Figure 10a. There is a prominent cloud feature in the northeast of the OLCI image with low cloud top pressure as well as low cloud base pressure. There are larger areas where CTP is less than 200 hPa.

The cloud optical thickness shows high variability in this area with quite low values. The values of the centre of gravity are more heterogeneous, indicating that the ice water content is in the more upper part of the cloud. But both quantities, the cloud base pressure and the centre of gravity, have to be interpreted with extremely carefulness (see Figure 10a). The information content of these measurements, or the degree of freedom (*DoF*), is estimated within the OCTPO2 retrieval scheme, described in the ATBD section 5.7 (Preusker and Fischer, 20121). It varies between 1.9 and 2.3 in the analysed OLCI scene, showing a significant increase in the region of lower cloud top pressure. The higher DoF values in the north-eastern part of the image points to higher variability in the cloud vertical profile. The cloud optical thickness is increased in this area as well (see Figure 10a, upper right).

Unfortunately, HALO did not fly into this area this day. There have been airborne measurements in the most westerly part of the OLCI swath (see the blue circle in Figure 10a/b). The cloud top pressure, derived from OLCI and WALES, agree well for optically thicker clouds. Again, partly filled pixels, which often occur when small cumulus is present, are interpreted with low cloud top pressure (see Figure 11).
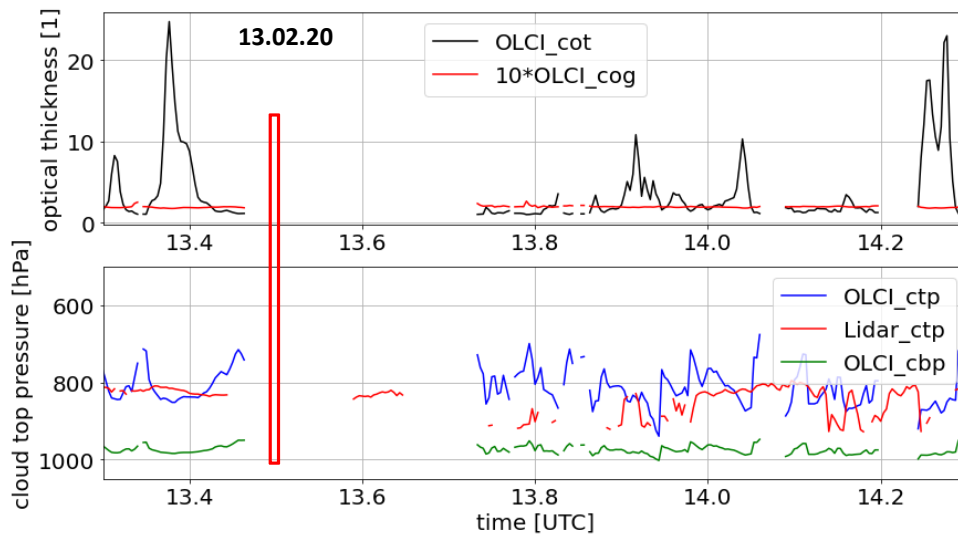
*Figure 11: Cloud top pressure (blue) and cloud base pressure (green) products derived from OLCI and WALES-Lidar (red) (lower Figure), cloud optical thickness and center of gravity as derived from OLCI (upper Figure) on the 13th of Feb. 2020; the overpass of Sentinel-3 is indicated as a red bar at 13:25 UTC.*

## 2.2   Validation of OLCI Cloud Properties with Ground-based Observations

Ground-based cloud-radar, micropulse lidar and ceilometer measurements, taken from the southern great plains ARM-site in Oklahoma are suitable for the validation of OLCI's cloud products. For the comparison of the ground- and satellite-based cloud products we chose the period of 26th of June 2020 to 1st of February 2021.

The ARM-site provides cloud observations from a Micropulse Lidar (http://dx.doi.org/10.5439/ 1508389), a Ka-band ARM Zenith Radar at 35 GHz (http://dx.doi.org/10.5439/1393438), and a ceilometer. The micropulse lidar (MPL) alone provides retrievals of the cloud-top and cloud-base pressure, which are also estimated from a combination of cloud-radar, micropulse and ceilometer measurements.

The matchups with OLCI observations have to fulfil the following criteria: 5x5 FR (Full Resolution) pixel collocated L1B- and L2- measurements within a time window of ± 6 minutes. Different criteria/filters are selected in the following analysis. Depending on the applied filter criteria 18 to 90 matchups could be realized. When no specific cloud filter is applied, 90 matchups could be identified within the considered period. The correlation between the cloud top pressure, derived from OLCI and micropulse lidar, is 0.52. while the use of a combination of radar-MPL-ceilometer measurements leads to a correlation of 0.59 (see Figure 12). There is quite a large spread with a root-mean-square-difference (rmsd) of ~200 hPa.

When the matchup conditions are more restricted, that cloud cover has to be >0.8 and the cloud optical thickness >3, the correlation increases to 0.87 for MPL data alone and 0.79 for all three combined ground-based measurements (Figure 13). The rmsd is also drastically reduced to 126 hPa.

When the criteria are even more restricted, a cloud fraction of >0.8 and clouds in a range of COT >3 and <30, (arbitrarily chosen to account for the low sensitivity of ground-based measurements of optically thick clouds) the correlation between OLCI and ground-truth CTP increases to 0.90, but the rmsd does not improve (*Figure 14*). While the combined CTP retrieval, based on radar-, MPL-, and ceilometer-measurements estimates lower CTP than the MPL retrieval alone, which might be caused by the fact that the lidar signal does not penetrate clouds with larger COT. The signal of a cloud radar

at 35 GHz is altered by cloud droplets but penetrates through clouds and detects also ice crystals at higher atmospheric layers.
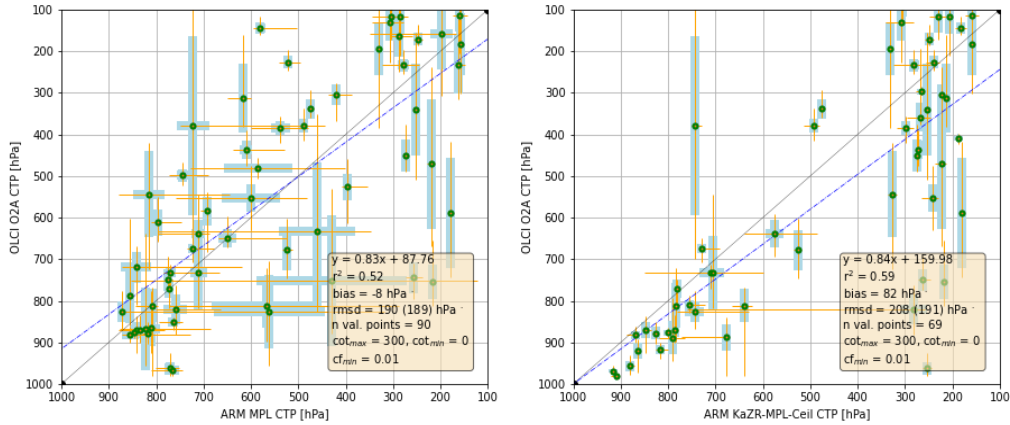


*Figure 12: Cloud top pressure (CTP) derived from ARM-site MPL (micropulse lidar) and OLCI (left), and combined radar-MPL-ceilometer against OLCI CTP (right); for more details see text.*
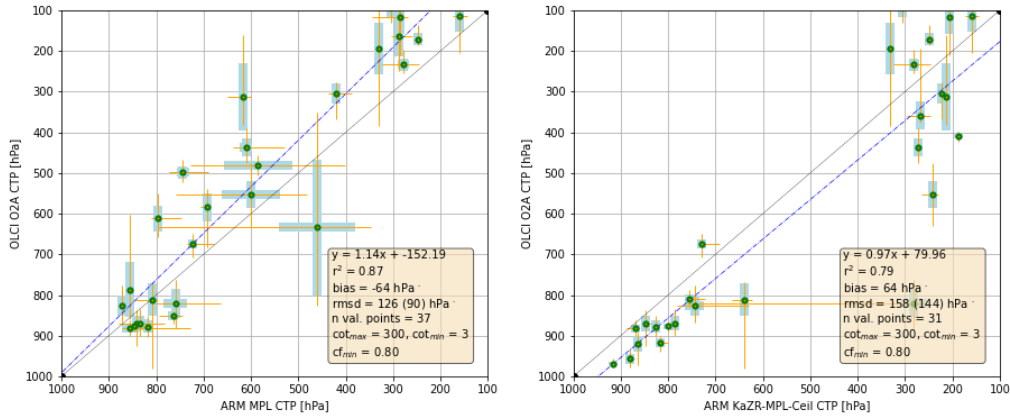


*Figure 13: As Figure 12, but only for cloud fraction > 0.8 and cloud optical thickness > 3; for more details see text.*
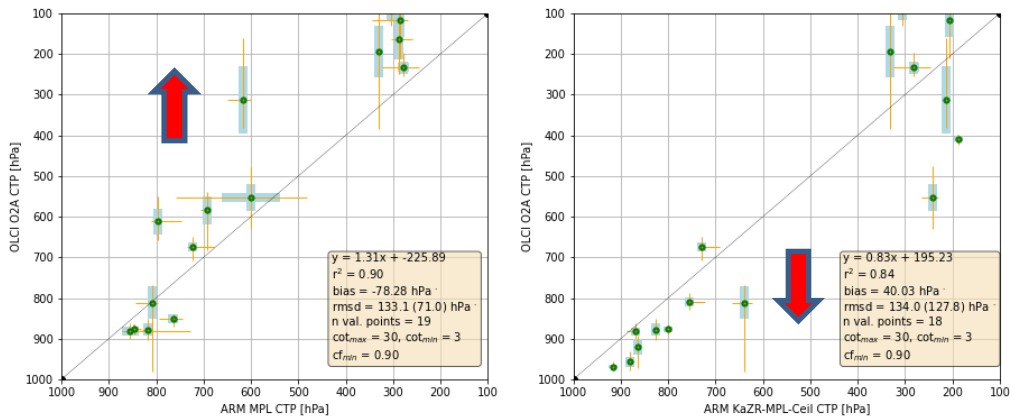


*Figure 14: As Figure 12, but only for cloud fraction > 0.8 and cloud optical thickness > 3 and <30; for more details see text.*

To better understand those features, both ground-based CTP products are compared to each other (*Figure 15*, right). For all clouds, up to COT of 300, the results differ with a rmsd=206 hPa and a low

correlation of 0.50. When the matchups are more restricted and only optically thinner clouds of maximum COT=10 are considered the relationship between both retrievals agree much better (*Figure 15*, left). This confirms the fact that the MPL does not see the cloud top pressure well under thick clouds.

A validation of OLCI's cloud geometrical thickness product is challenging but has been proved by using the MPL and the combined radar-MPL-ceilometer products (Figure 16). From MPL data alone we estimate CGT values between 0.1 and 0.5, from OLCI measurements we retrieve CGT between 0.4 and 0.8. In general, the cloud geometrical thickness with the OCTPO2 algorithm is overestimated.

The spread of CGT, estimated from radar-MPL-ceilometer data, is larger, which corresponds to the finding that also lower CTPs are retrieved from the combined dataset.
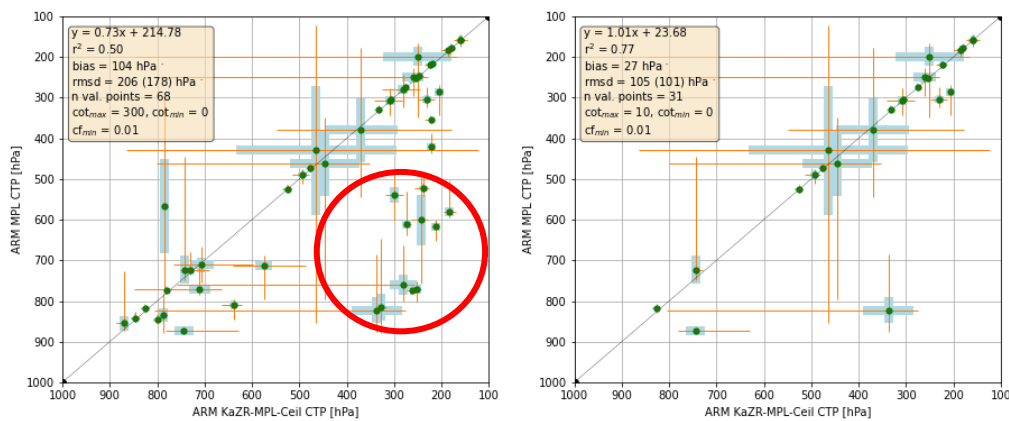


*Figure 15: Cloud top pressure (CTP) derived from ARM-site MPL (micropulse lidar) and combined radar-MPL-ceilometer for all clouds (left) and clouds with COT<10; for more details see text.*
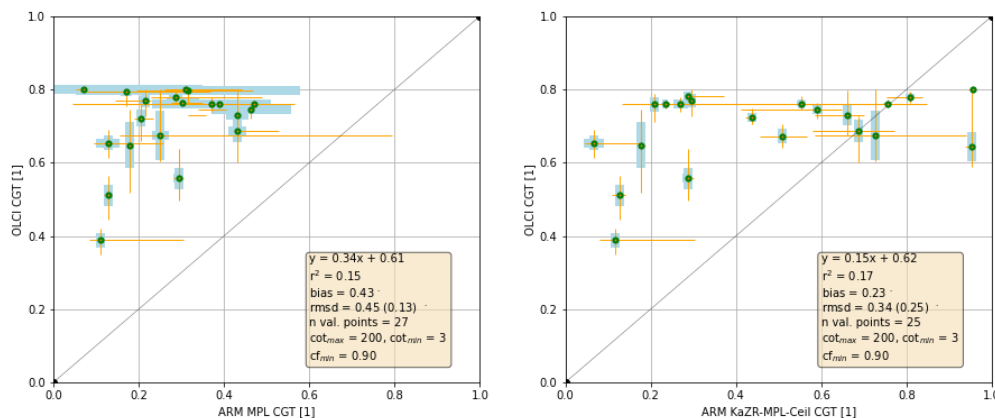


*Figure 16: Cloud geometrical thickness (CGT) derived from ARM-site MPL (micropulse lidar) and OLCI (left) as well as derived from combined radar-MPL-ceilometer (right); for more details see text.*

The OCTPO2 cloud base pressure (CBP) product is compared with the MPL alone and combined radar-MPL-ceilometer retrieval (Figure 17). For both validation datasets CBP is overestimated by OLCI for higher clouds. The OCTPO2 parameter of the centre of gravity (CoG), which is an expression for the vertical cloud structure, might compensate the effect of the geometrical thickness on OLCI O2 A-band measurements. At this stage, there are not enough cases to decide whether to constrain CGT or CoG. This decision depends also on the reliability of the auxiliary data, constraining the vertical profile of the clouds.
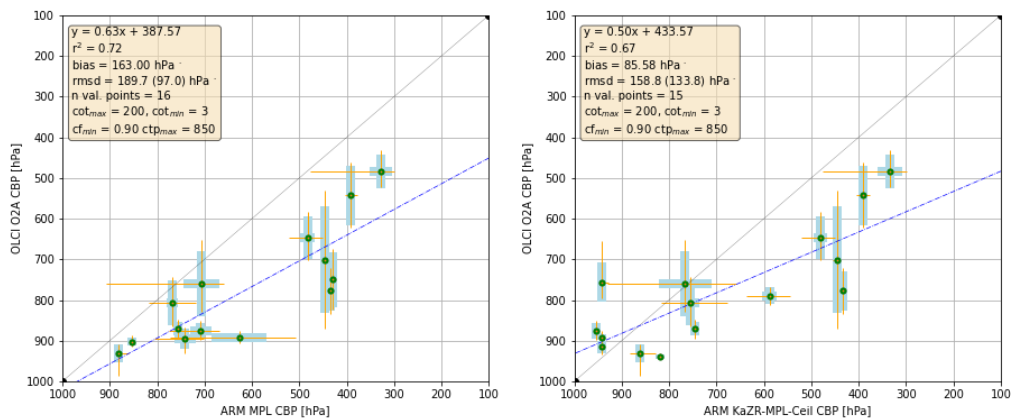
*Figure 17: Cloud base pressure (CBP) derived from ARM-site MPL (micropulse lidar) and OLCI (left) as well as derived from combined radar-MPL-ceilometer (right); only for clouds with COT>3 and CTP<850 hPa; for more details see text.*

## 2.3　Information Content of OLCI O2 A-band Measurements

The primary goal of the OCTPO2 retrieval algorithm is to detect the cloud top pressure from OLCI O2 A-band measurements. From previous studies, we know (Fischer et al., 1990; Preusker, 2002; Carbajal et al, 2014), that the penetration depth of the radiation in the $O_2$ absorption band depends on the vertical structure of the cloud. In particular, the cloud top pressure of thin cirrus or cirrus above clouds is overestimated. In the framework of this OCTPO2 project, we defined and developed a procedure to account for the vertical cloud structure by introducing two additional properties, the cloud geometrical thickness (CGT) and the center of gravity (CoG), beside the cloud top pressure and the cloud optical thickness. Unfortunately, there are only three OLCI measurements in the O2 A-band absorption and two just beside as reference, which limits the observed information content.

The information content of the measurements, or the degree of freedom (*DoF*) has been estimated from a set of OLCI scenes for the MSG disk on the 18th of February 2020 (see Figure 18). There are large areas which are dominated by only 2 independent properties, which could be retrieved. Above the Sahara Desert the *DoF* drops to less than 1.5 due the bright land surface and optically thin clouds. In the tropical regions we achieve values even higher than 2.5, which represent optical thick and vertical structured clouds.

The information content of the OLCI O2 A-band measurements is limited and even depends on the clouds themselves. In most cases there is not enough information to retrieve all cloud properties, COT, CTP, CGT and CoG.
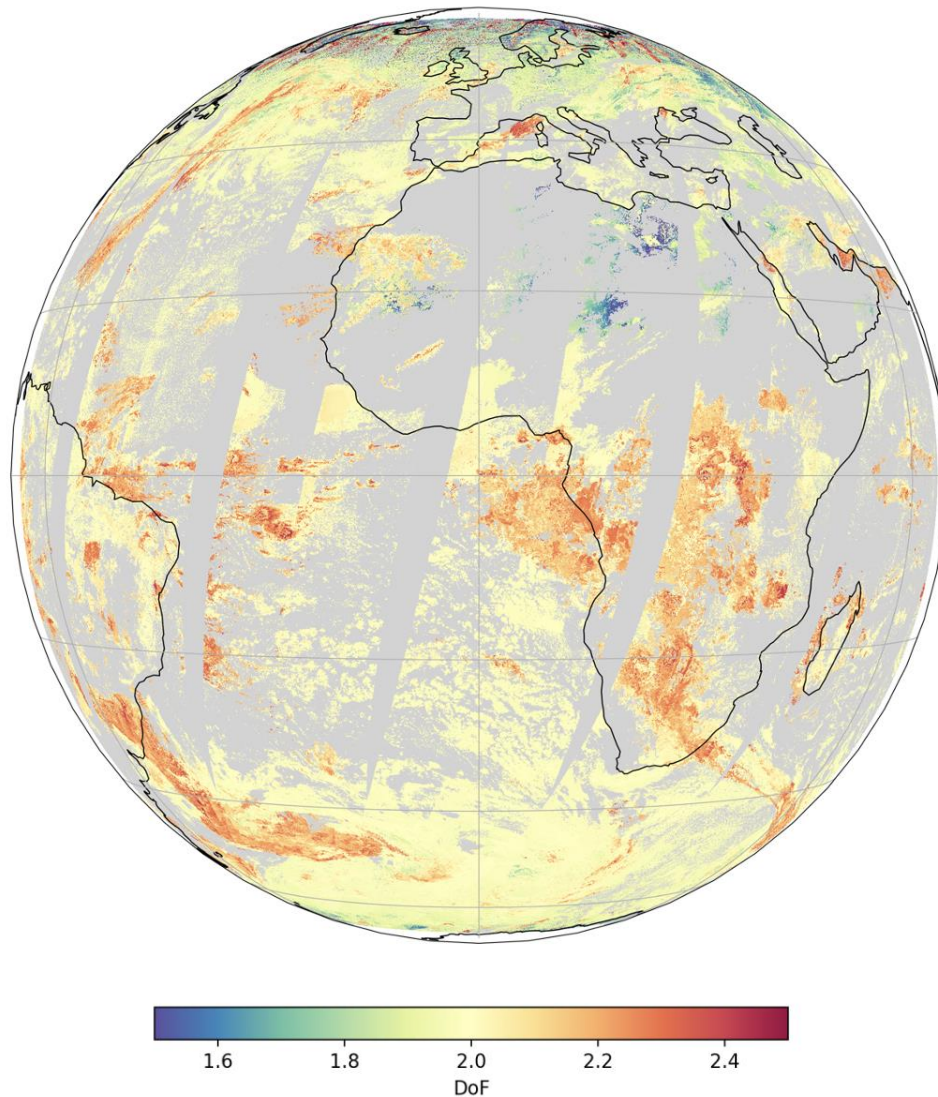
*Figure 18: Degree of freedom (DoF) as derived from OLCI on the 18th of Feb. 2020.*

## 2.4   Comparison between Cloud Top Pressure Derived from MODIS and OLCI

A comparison between two different cloud top pressure retrievals, the $CO_2$-slicing and the O2 A-band approach, gives further understanding of the capability of the OCTPO2 algorithm. The MODIS CTP retrieval is based on the $CO_2$-slicing technique, using six thermal infrared measurements along the shortwave shoulder of the 14 μm $CO_2$ absorption band between 11 and 14.2 μm (Menzel et al., 2008). Since the weighting functions for the $CO_2$ absorption bands on MODIS peak well into the troposphere, $CO_2$ slicing is most effective for the analysis of mid to high-level clouds, especially semitransparent clouds such as cirrus. Comparisons of MODIS CTP with airborne and satellite lidar retrievals are confirming, that the cloud top pressures are within 50 hPa in high, optically thin cirrus and midlevel water clouds. Also, in atmospheres prone to temperature inversions, the MODIS cloud algorithm places the cloud above the inversion and hence can be as much as 200 hPa off its true location (Menzel et al., 2008). For this comparison we used CTP products of the MOD06 and MYD06 version 6.01 (Ackerman et al., 2021).
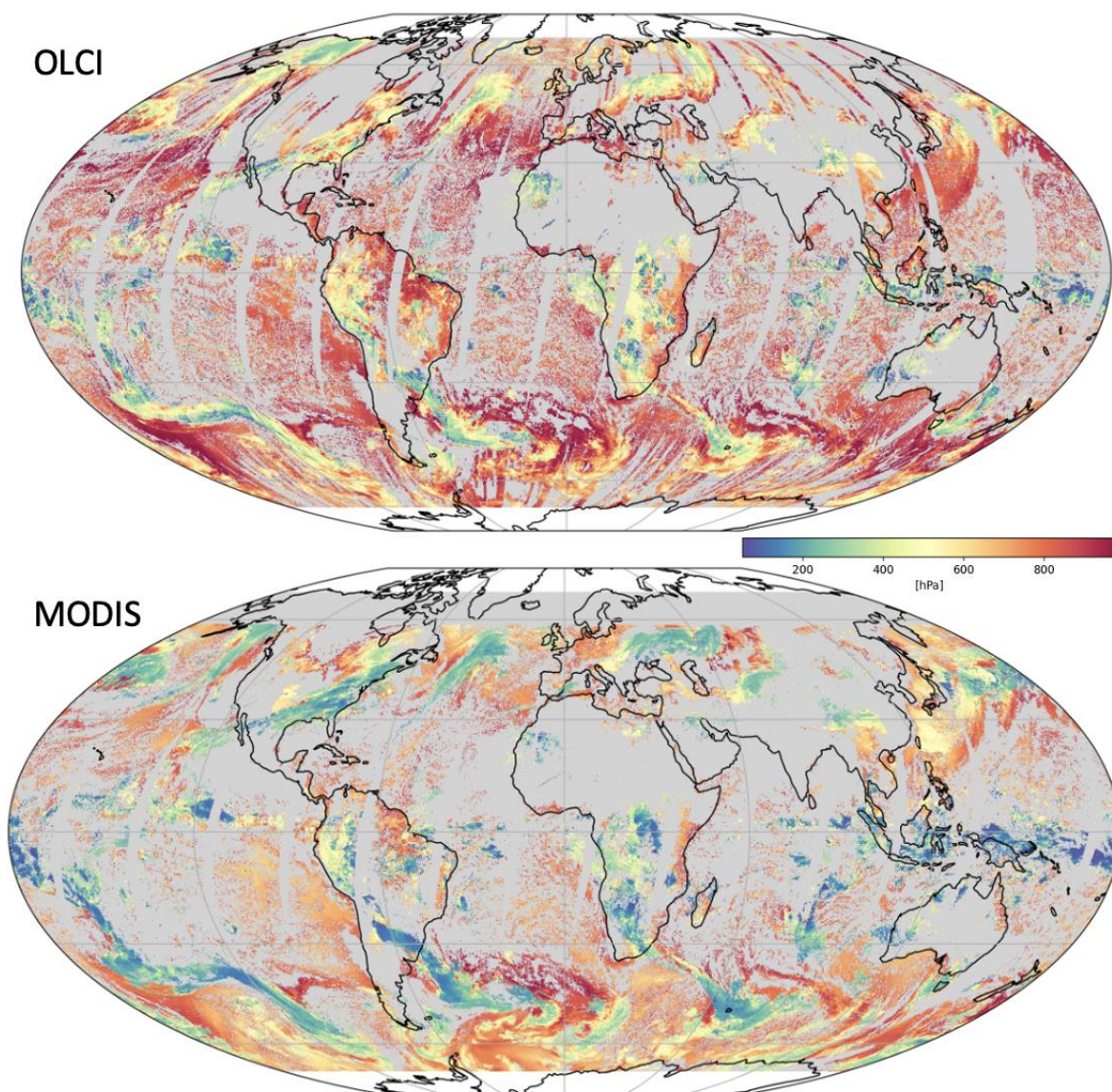
*Figure 19: Cloud top pressure derived from OLCI (upper) and MODIS (lower) for clouds with cot>5 on the 18th of Feb. 2020.*

A comparison of global MODIS and OLCI cloud top pressure retrievals on the 18th of February is shown in Figure 19. While the general cloud pattern is caught by both retrieval methods, it is obvious that MODIS retrieves higher clouds than OLCI. On the other side, MODIS seems to observe fewer low-level clouds. Those findings are consistent with the result of the MODIS cloud top pressure algorithm description as given in detail by Menzel et al. (2008).

To further analyze the differences in both retrievals, we looked at the histograms of the estimated cloud top pressure only for clouds with an optical thickness higher than 5 and 25 (Figure 20). When all clouds with COT>5 are considered, we found a correlation of 0.55, a bias of 97 hPa, and a bias-corrected rmsd of 164 hPa. The number of estimated CTP retrievals is displayed for MODIS and OLCI in Figure 20 as well, showing even more clearly that OLCI observes more low-level clouds, while MODIS detects more high-level clouds. When only clouds with COT>25 are compared, the correlation between both retrievals increases to 0.64. The linear relationship between both cloud top pressure products is

visible, showing that OLCI is sensitive to different parts of the cloud compared to MODIS. Those results are also found for other days of the year, thus the general conclusion is valid for different seasons.
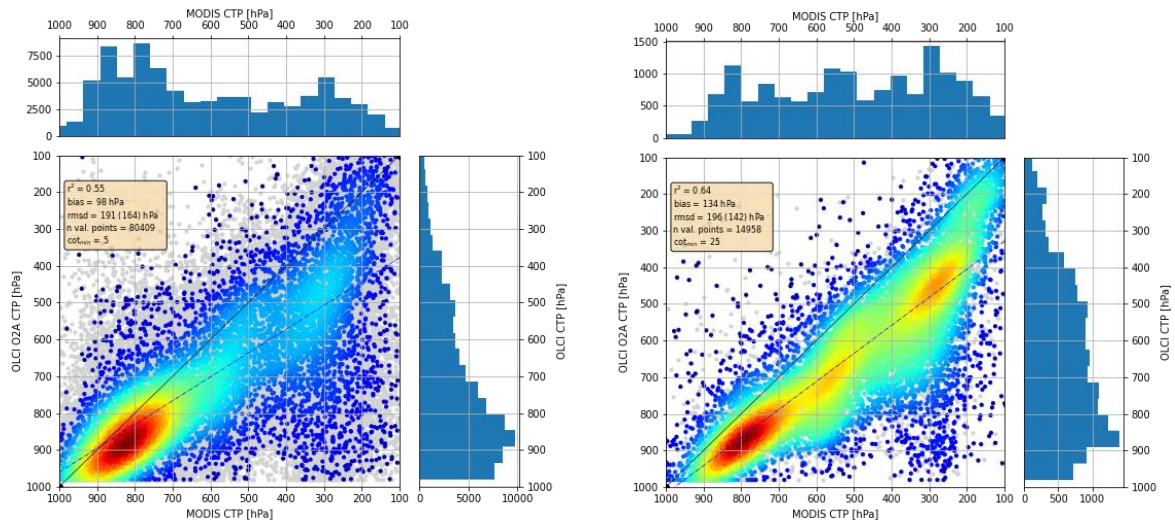


*Figure 20: Histogram of cloud top pressure derived from OLCI and MODIS for clouds cot>5 (left) and cot>25 (right) on the 18th of Feb. 2020.*

# 3  Conclusions and Recommendations

This validation exercise comprises a variety of measurements, based on ground-based cloud radar, micropulse and ceilometer instruments as well as air-borne lidar, which are used to estimate the accuracy of OLCI's OCTPO2 cloud products.

A thorough validation of the OCTPO2 cloud products is difficult because the different cloud observing instruments are sensitive to different cloud properties, mainly driven by droplet size and droplet density. Additionally, clouds vary fast in time and the collocation of the different observations are highly complex and limited in terms of accuracy.

Following the airborne lidar measurements we found generally a good agreement with the cloud top pressure, derived from OLCI. We further learned that the retrieval of CTP is more accurate with higher cloud optical thickness which should be larger than 2-3. The estimated cloud geometrical thickness and centre of gravity seem to be reasonable, but the observed clouds are limited to the lower part of the atmosphere. Following the analysis of the information content, we expect in most of the cases only 2 independent pieces of information.

The ARM-site cloud observations contribute to a better understanding of the validity of the retrieved OCTPTO2 products. The root mean square differences between the OLCI and ground-based derived cloud top pressure is within 130 hPa when the cloud cover is higher than 80% and the optical thickness larger than 3.

The comparison of cloud top pressure retrievals from OLCI and MODIS measurements provides us with a global view of different cloud types and regimes. While OLCI is based on the interaction of scattered and absorbed radiation within clouds, MODIS observes emitted radiation, which is already more sensitive to thinner and colder clouds. We found that MODIS observes more mid- and high-level clouds, while OLCI is more sensitive to low-level clouds. In general, OLCI overestimates the cloud top pressure for mid- and high-level clouds when compared to MODIS CTP retrievals.

Following the results of the validation study, we conclude that the required accuracy of 0.5 km in the cloud top height for applications in *High Resolution NWP*, as discussed in Preusker and Fischer (2021), is achieved in most of the cases, knowing that OCTPO2 still estimate high clouds to low. In cases of a perfect match between airborne lidar and OCLI we already estimated the cloud top heights within 200 m by both observations.

We recommend further activities to foster the evolution of the OCTPO2 retrieval. These are:

- o Introducing a procedure to estimate apriori values for CoG and CGT, which could be based on temperature and humidity profiles, as provide by ECMWF forecasts and part of the L1 OLCI and SLSTR data files. Detailed studies are needed to quantify the according uncertainties.
- o Improvement of the OCTPO2 algorithm by adding thermal measurements from SLSTR.
- o Further validation studies, including radiative transfer simulations with a focus on higher spectral resolution, to benefit from the upcoming FLEX mission, which will fly in convoy with a Sentinel-3 satellite and provide high spectral resolution measurements in the $O_2$ A-band.
- o Further validation by the use of ground-based cloud radar measurements as well as air-borne campaigns.

The new OCTPO2 algorithm has fundamental advantages and is expandable to use additional thermal infrared bands of SLSTR. Further on, the OCTPO2 algorithm provides consistent retrievals for current instruments (OLCI and TROPOMI) and future operational instruments such as METImage.

# References

Ackerman, S., P. Menzel, and R. Frey, 2021: Terra Product Descriptions: MOD06_L2 - Cloud Top Properties. http://dx.doi.org/10.5067/MODIS/MOD06_L2.061.

Bennartz, R. and J. Fischer, 2000: A modified k-distribution approach applied to narrow band water vapour and oxygen absorption estimates in the near infrared. Journal of Quantitative Spectroscopy & Radiative Transfer, 66:539–553.

Carbajal-Henken, C., R. Lindstrot, F. Filipitsch, A. Walther, J. Fischer, 2012: FAME-C: Retrieval of Cloud Top Pressure with Vertically Inhomogeneous Cloud Profiles, Proc. International Radiation Symposium 2012, Berlin, Germany, 06-10 August 2012.

Carbajal Henken, C. K., Lindstrot, R., Preusker, R., and Fischer, J., 2014: FAME-C: cloud property retrieval using synergistic AATSR and MERIS observations, Atmos. Meas. Tech. Discuss., 7, 4909-4947, doi:10.5194/amtd-7-4909-2014.

Delwart S., R. Preusker, L. Bourg, R. Santer, D. Ramon, J. Fischer, 2006: MERIS in flight spectral calibration. Int. J. Remote Sensing, 28, 479-496.

Doppler, L., R. Preusker, R. Bennartz, J. Fischer, 2013: k-bin and k-IR: k-distribution methods without correlation approximation for non-fixed instrument response function and extension to the thermal infrared. Journal of Quantitative Spectroscopy and Radiative Transfer, 09 / 2013.

Drouin, B. J., D. C. Benner, L. R. Brown, M. Cich, T. Crawford, V. M. Devi, A. Guillaume, J. T. Hodges, E. J. Mlawer, D. Robichaud, F. Oyafuso, V. H. Payne, K. Sung, E. Wishnow, S. Yu, 2017: Multi-spectrum analysis of the oxygen A band. JQSRT, 186, 118–138.

Fischer, J. 1988: High Resolution Spectroscopy for Remote Sensing of Physical Cloud Properties and Water Vapour. In: Current Problems in Atmospheric Radiation, Ed. Lenoble and Geleyn, Deepak Publishing, 151-156.

Fischer, J. and H. Grassl, 1990: Detection of Cloud-Top Height from Backscattered Radiances within the Oxygen A-Band - Part 1: Theoretical Study.- J. Appl. Met., 30, 1245-1259.

Fischer, J., W. Cordes, A. Schmitz-Peiffer, W. Renger and P. Mörl, 1990: Detection of Cloud-Top Height from Backscattered Radiances within the Oxygen A-Band - Part 2: Measurements. J. Appl. Met., 30, 1260-1267.

Gordon, I.E., L.S. Rothman, C. Hill, R.V. Kochanov, Y. Tan, P.F. Bernath, M. Birk, V. Boudon, A. Campargue, K.V. Chance, B.J. Drouin, J.-M. Flaud, R.R. Gamache, J.T. Hodges, D. Jacquemart, V.I. Perevalov, A. Perrin, K.P. Shine, M.-A.H. Smith, J. Tennyson, G.C. Toon, H. Tran, V.G. Tyuterev, A. Barbe, A.G. Csaszar, V.M. Devi, T. Furtenbacher, J.J. Harrison, J.-M. Hartmann, A. Jolly, T.J. Johnson, T. Karman, I. Kleiner, A.A. Kyuberis, J. Loos, O.M. Lyulin, S.T. Massie, S.N. Mikhailenko, N. Moazzen-Ahmadi, H.S.P. Muller, O.V. Naumenko, A.V. Nikitin, O.L. Polyansky, M. Rey, M. Rotger, S.W. Sharpe, K. Sung, E. Starikova, S.A. Tashkun, J. Vander Auwera, G. Wagner, J. Wilzewski, P. Wcislo, S. Yu, E.J. Zak, 2017: The HITRAN2016 Molecular Spectroscopic Database. Journal of Quantitative Spectroscopy and Radiative Transfer, ISSN 0022-4073, DOI 10.1016/j.jqsrt.2017.06.038.

Hollstein, A. and J. Fischer, 2012: Radiative transfer solutions for coupled atmosphere ocean systems using the matrix operator technique. Journal of Quantitative Spectroscopy & Radiative Transfer, 113: 536–548.

Hollstein, A., J. Fischer, C. Carbajal Henken, and R. Preusker, 2015: Bayesian cloud detection for MERIS, AATSR, and their combination, Atmospheric Measurement Techniques 8, 1757-1771.

Koelemeijer, R. B. A., P. Stammes, J. W. Hovenier, and J. F. de Haan (2001), A fast method for retrieval of cloud parameters using oxygen A band measurements from GOME, J. Geophys. Res., 106, 3475-3490.

Kollewe, M., and J. Fischer, 1994: Definition of the oxygen A-band channels of ENVISAT's Medium Resolution Imaging Spectrometer for cloud monitoring, Proc. SPIE 2309, Passive Infrared Remote Sensing of Clouds and the Atmosphere II, (23 December 1994); doi: 10.1117/12.196677.

Kokhanovsky, A. A., J. L. Deuzé, D. J. Diner, O. Dubovik, F. Ducos, C. Emde, M. J. Garay, R. G. Grainger, A. Heckel, M. Herman, I. L. Katsev, J. Keller, R. Levy, P. R. J. North, A. S. Prikhach, V. V.

Lindstrot, R. and R. Preusker, 2012: On the efficient treatment of temperature profiles for the estimation of atmospheric transmittance under scattering conditions. Atmospheric Measurement Techniques, 5: 2525–2535.

Lindstrot, R., R. Preusker, H. Diedrich, L. Doppler, R. Bennartz, and J. Fischer, 2012: 1D-Var retrieval of daytime total columnar water vapour from MERIS measurements. Atmospheric Measurement Techniques, 5: 631–646.

McClatchey, R., R. Fenn, J. Selby, F. Volz, and J. Garing, 1972: Optical properties of the atmosphere (3rd ed.). Technical report, Air Force Cambridge Research Laboratories.

Menzel, P., R. Frey, H. Zhang, D. Wylie, C. Moeller, R. Holz, B. Maddux, B. Baum, K. Strabala, and L. Gumley, 2008: MODIS Global Cloud-Top Pressure and Amount Estimation: Algorithm Description and Results. Jour. of Applied Met. and Climate, p. 1175-1198., 2008.

Mlawer, E. J., Payne V. H., Moncet, J., Delamere, J. S., Alvarado, M. J., and Tobin, D.C., 2012: Development and recent evaluation of the MT_CKD model of continuum absorption, Philos. T. R. Soc. A, 370, 2520–2556, https://doi.org/10.1098/rsta.2011.0295, 2012.

Naud, C, J.-P. Muller, B. Baum, R. Bennarzt, R. Frey, P. Menzel, H. Zhang, J. Fischer, R. Preusker, 2004: Inter-comparison of MERIS, MODIS and MISR cloud top heights. In: European Space Agency, (Special Publication) ESA SP (pp. 19 - 24).

Preusker, R., and J. Fischer, 2021: Cloud Top Pressure development from Sentinel-3 OLCI project OCTPO2 – ATBD. EUMETSAT.

Preusker, R., and R. Lindstrot, 2009: Remote Sensing of Cloud-Top Pressure Using Moderately Resolved Measurement within the Oxygen A Band—A Sensitivity Study. J. Applied Meteoro. Climatology, 48, 1564-1574.

Preusker, R., J. Fischer, A. Hünerbein, C. Brockmann, M. Zühlke, and U. Krämer, 2008: Improved MERIS cloud detection. In Lacoste, H. and Ouwehand, L., editors, Proceedings of the 2nd MERIS/(A)ATSR Workshop, pages CD–Rom, Frascati, Italy. ESA SP-666, ESA Publications Division.

Ptashnik I.V., K.P. Shine, A.A. Vigasin, 2011: Water vapour self-continuum and water dimers: 1. Analysis of recent work. J. of Quant Spect. and Rad. Trans. 112(8); 1286-303.

Richardson, Mark and Graeme L. Stephens, 2018: Information content of OCO-2 oxygen A-band channels for retrieving marine liquid cloud properties, Atmos. Meas. Tech., 11, 1515–1528.

Rodgers, C., 2000: Inverse Methods for Atmospheric Sounding: Theory and Practice. World Scientific Pub Co.

Wiscombe, W.J., 1980: Improved Mie scattering algorithms. Applied Optics 19: 1505– 1509.